JOURNAL OF GEOPHYSICAL RESEARCH, VOL. 114, G04022, doi:10.1029/2009JG001095, 2009

Projected changes in atmospheric heating due to changes in fire disturbance and the snow season in the western Arctic, 2003–2100

E. S. Euskirchen,[1] A. D. McGuire,[2] T. S. Rupp,[3] F. S. Chapin III,[1] and J. E. Walsh[4]

Received 7 July 2009; accepted 10 September 2009; published 18 December 2009.

[1] In high latitudes, changes in climate impact fire regimes and snow cover duration, altering the surface albedo and the heating of the regional atmosphere. In the western Arctic, under four scenarios of future climate change and future fire regimes (2003–2100), we examined changes in surface albedo and the related changes in regional atmospheric heating due to: (1) vegetation changes following a changing fire regime, and (2) changes in snow cover duration. We used a spatially explicit dynamic vegetation model (Alaskan Frame-based Ecosystem Code) to simulate changes in successional dynamics associated with fire under the future climate scenarios, and the Terrestrial Ecosystem Model to simulate changes in snow cover. Changes in summer heating due to the changes in the forest stand age distributions under future fire regimes showed a slight cooling effect due to increases in summer albedo (mean across climates of -0.9 W m^{-2} decade^{-1}). Over this same time period, decreases in snow cover (mean reduction in the snow season of 4.5 d decade^{-1}) caused a reduction in albedo, and a heating effect (mean across climates of 4.3 W m^{-2} decade^{-1}). Adding both the summer negative change in atmospheric heating due to changes in fire regimes to the positive changes in atmospheric heating due to changes in the length of the snow season resulted in a 3.4 W m^{-2} decade^{-1} increase in atmospheric heating. These findings highlight the importance of gaining a better understanding of the influences of changes in surface albedo on atmospheric heating due to both changes in the fire regime and changes in snow cover duration.

Citation: Euskirchen, E. S., A. D. McGuire, T. S. Rupp, F. S. Chapin III, and J. E. Walsh (2009), Projected changes in atmospheric heating due to changes in fire disturbance and the snow season in the western Arctic, 2003–2100, *J. Geophys. Res.*, *114*, G04022, doi:10.1029/2009JG001095.

1. Introduction

[2] Warming is projected to be greater at high latitudes than other parts of the globe, with increases ranging 1.5–4.5°C of the projected global mean, and substantial drying expected in the continental interior by 2100 [*Flannigan et al.*, 2005; *Christensen et al.*, 2007]. This warming may impact both the wildfire regimes in the Canadian and Alaskan western Arctic [*Kasischke et al.*, 2002, 2003; *Duffy et al.*, 2005; *Flannigan et al.*, 2005] and the duration of the period of snow covered ground in this region [*Dye*, 2002; *Stone et al.*, 2002; *Chapin et al.*, 2005; *Euskirchen et al.*, 2006, 2007]. Changes in boreal forest fire regimes and the snow season have substantial implications for changes in feedbacks between these high-latitude ecosystems and the climate system [*McGuire and Chapin*, 2006; *Randerson et al.*, 2006; *Euskirchen et al.*, 2007].

[3] Wildfire is the dominant disturbance regime of the boreal forests in the western Arctic, with much of this area subject to short fire return intervals of 50–150 years [*Payette*, 1992]. This creates a mosaic of stand ages across the landscape, with each forest stand representing a specific postfire successional stage. An increased frequency of years with large fires from the 1960s to the 1990s has tripled the area burned in the North American boreal forest region [*Kasischke and Turetsky*, 2006], leading to a landscape with a large proportion of young stands. This increased frequency is thought to be due to greater midsummer drought stress in conifer ecosystems [*Welp et al.*, 2007] and to a lengthening of the summer fire season [*Wotton and Flannigan*, 1993; *Stocks et al.*, 1998; *Westerling et al.*, 2006]. These changes in fire frequency and area burned influence biosphere-atmosphere energy exchange at regional and continental scales [*Chambers et al.*, 2005; *Amiro et al.*, 2006; *Randerson et al.*, 2006].

[4] Fire in the boreal forest often causes stand-replacing mortality, opening closed canopies, and immediately impacting the surface albedo and energy balance. These impacts can last for decades after the initial disturbance. The first year following fire is marked by a low value of summer albedo similar to that found in mature coniferous forests due

[1] Institute of Arctic Biology, University of Alaska Fairbanks, Fairbanks, Alaska, USA.
[2] Alaska Cooperative Fish and Wildlife Unit, U.S. Geological Survey, University of Alaska Fairbanks, Fairbanks, Alaska, USA.
[3] Department of Forest Sciences, University of Alaska Fairbanks, Fairbanks, Alaska, USA.
[4] International Arctic Research Center, University of Alaska Fairbanks, Fairbanks, Alaska, USA.

0148-0227/09/2009JG001095$09.00

to black carbon on the surface caused by the fire [*Chambers et al.*, 2005; *Amiro et al.*, 2006; *Randerson et al.*, 2006]. Subsequently, an herbaceous ground cover begins to grow during the summer, causing the value of summer albedo to increase. During the period of snow covered ground in the first years following fire, the open surface has a high value of albedo [*Liu et al.*, 2005; *Amiro et al.*, 2006; *Liu and Randerson*, 2008]. Latent and sensible heat fluxes remain lower in the recently burned areas (e.g., <10 years postburn) compared to those dominated by mature forest. This is due to decreases in net radiation in the recently burned areas which are caused by a decrease in surface roughness and turbulent exchange due to the loss of canopy structure [*Chambers et al.*, 2005; *Liu et al.*, 2005; *Liu and Randerson*, 2008].

[5] As the forest continues to recover in the years following fire, a mixture of deciduous shrubs (e.g., willow) and trees (e.g., aspen, birch) establishes. The summer albedo in these deciduous ecosystems is generally greater than in the coniferous ecosystems that dominate the final successional stage of postfire recovery [*Liu et al.*, 2005; *Amiro et al.*, 2006; *Liu and Randerson*, 2008]. The albedo during the snow season in these deciduous stands is generally lower than during the years immediately following fire, but greater than in the coniferous ecosystems. In summer, canopy conductance and evapotranspiration rates are higher than in both the recently burned stands and the coniferous sites [*Baldocchi et al.*, 2000; *Liu et al.*, 2005; *Liu and Randerson*, 2008]. Therefore, a greater percent of net incoming radiation is transferred as latent heat, with a parallel decrease in sensible heat. At the landscape-to-regional scale, an increase in fire frequency and area can lead to an overall increase in albedo and decrease in sensible heating due to an increase in young deciduous stands. This negative feedback to radiative forcing (-4.2 W m^{-2} for the global atmosphere [*Randerson et al.*, 2006]) has been shown to be larger than the positive feedback from fire emitted greenhouse gases over the course of an 80 year fire cycle ($+1.6$ W m^{-2} global average [*Randerson et al.*, 2006]). Gaining a better understanding of how the age structure of forest ecosystems across landscapes and regions may change under future fire regimes is paramount in predicting future changes in surface albedo and regional atmospheric heating.

[6] In contrast to this negative climate feedback from an increase in fire frequency and area, a positive feedback to atmospheric heating may occur due to a decrease in the period of snow covered ground that is observed and expected under a warming climate [*Dye*, 2002; *Euskirchen et al.*, 2006, 2007, 2009]. Snowmelt in northern Alaska occurred approximately 2.5 d decade^{-1} earlier during the last several decades of the twentieth century [*Stone et al.*, 2002; *Chapin et al.*, 2005; *Euskirchen et al.*, 2007], while the return of snowfall occurred approximately 1.2 d decade^{-1} later during this same period [*Euskirchen et al.*, 2007]. This retreat of snow is important due to the resulting feedback: as snow retreats, less solar energy is reflected to space, and more energy is absorbed and transferred to the atmosphere [*Groisman et al.*, 1994], causing a positive snow/albedo feedback loop that reinforces warming. A previous study [*Euskirchen et al.*, 2007] found that these recent changes in the timing of snowmelt in the spring and return of snow in the fall resulted in an increase in atmospheric heating of 2–3 W m^{-2} decade^{-1} in the western Arctic from 1970–2000. The magnitude of this increase in atmospheric heating due to decreases in snow cover suggests that it is important to continue to monitor and use models to predict these changes in snow cover and atmospheric feedbacks.

[7] Based on these potential negative feedbacks to atmospheric heating under increased fire frequency and area burned versus the positive feedbacks to atmospheric heating under a shortening of the snow season, we ask the following questions: (1) What is the relative effect on land surface albedo and atmospheric heating due to changes in forest stand age distribution under future fire regimes, (2) What is the relative effect on land surface albedo and atmospheric heating due to future changes in snow cover, (3) What is the relative effect on atmospheric heating due to changes in snow cover and vegetation (e.g., do these effects cancel each other out), and (4) How do different parameterizations of the changes in albedo (e.g., remotely sensed versus observational) over the course of forest succession impact the estimates of atmospheric heating? We base our analyses on projected ecosystems in the western Arctic (Figure 1) between the years 2003–2100.

2. Methods

2.1. Overview

[8] We performed model simulations for 2003–2100 at a 1 by 1 km spatial resolution in the western Arctic. We use a transient landscape-level model of vegetation dynamics, the Alaskan Frame-based Ecosystem Code (ALFRESCO), to estimate the changes in burn area and the corresponding changes in the distribution of the ages of the ecosystems postfire in the study region. We used the water balance and irradiance modules within the Terrestrial Ecosystem Model (TEM) to calculate changes in the length of the snow season and incoming solar irradiance and longwave radiation. We calculated changes in albedo due to summer and snow season changes in the land surface based on two different types of albedo estimates, those from a synthesis of empirical field-collected albedo measurements [*Amiro et al.*, 2006] and those based on remotely sensed data [*Randerson et al.*, 2006; *Lyons et al.*, 2008]. We then computed changes in atmospheric heating in the western Arctic due to changes in the age structure of the ecosystems postfire and due to changes in the length of the snow season.

2.2. Study Region

[9] For this study, we chose the western Arctic as the spatial domain (Figure 1), an area encompassing the entire Yukon River drainage basin and the surrounding regions (220 million ha total land area, with 35,365,300 ha forested area). The domain includes all of Alaska (except the extreme southeastern panhandle and the Aleutian Islands), the Yukon Territory, and portions of British Columbia and the Northwest Territories. This region contains strong gradients in climate, vegetation, topography, and parent material. While this area does contain tundra which may burn, historical fire within this region is restricted almost exclusively to boreal forest within the more continental interior regions (Figure 1) [see also *McGuire et al.*, 2008]. In the

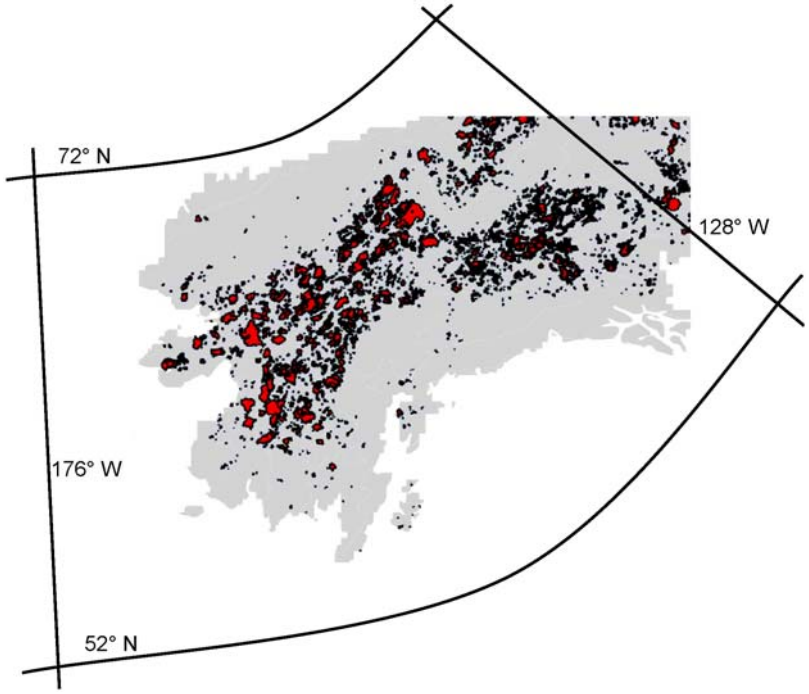

Figure 1. Map of the study domain, the western Arctic, and the perimeters of large fires between 1950 and 2000.

application presented here, we assume that the tundra area does not burn, and that all fires were due to natural causes (e.g., lightning ignitions) since the human caused fires in the region are locally associated with human activity in a region of low population density [*Calef et al.*, 2008], with the number of large fires (>10,000 ha) remaining relatively constant since the 1950s (E. S. Kasischke et al., Alaska's changing fire regime: Implications for the vulnerability of its boreal forests, submitted to *Canadian Journal of Forest Research,* 2009). From 1950 to 2000, the interannual variability in the total area burned within this region is large, ranging from a minimum of 1,600 ha to a maximum of 2,331,000 ha, with a mean of 426,000 ha (see Figure 2 in the work of *Rupp et al.* [2007]).

2.3. ALFRESCO Model

[10] ALFRESCO was originally developed to simulate the response of subarctic vegetation to a changing climate and disturbance regime [*Rupp et al.*, 2000a, 2000b]. Previous research has highlighted both direct and indirect (through changes in fire regime) effects of climate on the expansion rate, species composition, and extent of tree line in Alaska [*Rupp et al.*, 2000a, 2001]. Additional research, focused on boreal forest vegetation dynamics, has emphasized that fire frequency changes, both direct (climate driven or anthropogenic) and indirect (as a result of vegetation succession and species composition), strongly influence landscape-level vegetation dynamics and associated feedbacks to future fire regime [*Rupp et al.*, 2002; *Chapin et al.*, 2003]. Here, we focus our description of ALFRESCO on the fire routine [*Rupp et al.*, 2007] and successional dynamics.

[11] ALFRESCO is a state-and-transition model of successional dynamics that explicitly represents the spatial process of fire and vegetation recruitment across the landscape [*Rupp et al.*, 2000b]. ALFRESCO operates on an annual time step at a 1 km by 1 km pixel resolution to incorporate climate-fire-vegetation dynamics and facilitate the incorporation of regional climate data. ALFRESCO does not model fire behavior, but rather models the empirical relationship between monthly climate variables and flammability of a given cell in a manner that is consistent with the relationship described by *Duffy et al.* [2005]. The computation of the rate at which tundra and deciduous, white, and black spruce stands burned is based on *Starfield and Chapin* [1996] and *Cumming* [2001]. Fires are stochastically ignited and then burned recursively. The fire routine in ALFRESCO generates patterns of fire on the landscape that are consistent with the frequency, size distribution, and footprint of fire on the landscape that have been observed in the historical record since 1950. The primary source of uncertainty with respect to the simulation of fires on the landscape is the location, and this is driven by the stochasticity of ignition in both space and time. Because of this stochasticity, ensembles of model realizations are performed and analyzed. ALFRESCO also models the changes in vegetation flammability that occur during succession through a flammability coefficient that changes with vegetation type (e.g., deciduous forests are less flammable than coniferous forests) and stand age (i.e., succession [*Chapin et al.*, 2003]). Previous studies using ALFRESCO to estimate historical fire regimes have agreed well with observational data of annual area burned in the western Arctic [*Rupp et al.*, 2007].

[12] In the application of ALFRESCO presented here, fire and changes in ecosystem age structure due to fire disturbance for the years 1900–2100 were simulated annually at a 1 km by 1 km spatial resolution over the forested area in the

western Arctic. A 500 year spin-up was performed to permit realistic patch size and age-class distributions to be generated over multiple fire cycles [*Rupp et al.*, 2007]. The 500 yr time period is used because it represents at least a doubling of the length of the longest reported fire frequency for these ecosystem types (30–200 years [*Yarie*, 1981; *Van Cleve et al.*, 1991; *Chapin et al.*, 2003]). The analysis described here focuses on the years 2003–2100. Simulations for the years 2003–2100 were based on a range of future climates (described in section 2.7 below).

2.4. Snow and Solar Irradiance in the Terrestrial Ecosystem Model

[13] The Terrestrial Ecosystem Model contains a hydrology module and a radiation module that we use for calculating changes in the snow season and changes in incoming shortwave solar radiation as well as incoming and outgoing longwave radiation. The hydrology module of TEM, which is based on that of *Vörösmarty et al.* [1989], includes an algorithm to estimate the date of snowmelt (or snow return) from the monthly estimates of snowpack using a "ramp" between the monthly temperatures [*Euskirchen et al.*, 2007]. This algorithm linearly interpolates data for monthly air temperature across the month(s) preceding snowmelt (or snow return), the month of snowmelt (or snow return), and the month following snowmelt (or snow return). For example, to calculate the date of snowmelt when all snow has disappeared by April, approximately 30 points are interpolated between mean monthly March and April air temperature to determine the 15 points for the first half of April, and approximately 30 points are interpolated between mean monthly air temperature in April and May to determine the 15 points for the second half of April. The length of the snow-free season is calculated by subtracting the date of snowmelt from the date of snow return. As discussed by *Euskirchen et al.* [2006, 2007], the model estimates of the spatial extent and the temporal dynamics of snow cover are in agreement with those of *Dye* [2002].

[14] We calculated seasonal values of shortwave incoming solar irradiance (R_{Sin}) as well as incoming and outgoing longwave radiation in TEM for each half-degree grid cell. The estimates of shortwave incoming solar irradiance are based on the methodology of *Turton* [1986] and are attenuated by the input cloud cover with a correction based on that described by *Chang* [1968]. The values of longwave radiation, including incoming longwave radiation (R_{Lin}), outgoing longwave radiation (R_{Lout}), and net longwave radiation (R_{Lnet}), are based on *Idso and Jackson* [1969], and include a cloud correction factor [*Parkinson and Washington*, 1979]. The outgoing longwave radiation is calculated taking into account the fractional vegetation types in a given grid cell and the emissivity values for the given snow and nonsnow covered vegetation type, including deciduous forest, coniferous forest, and open canopy (e.g., recent burn [*Geiger et al.*, 2009]).

[15] We performed model simulations with the same transient climate data used in ALFRESCO (described in section 2.7) for the years 1901–2100 and analyzed the output data for the period from 2003 to 2100. To initialize the simulation, we ran TEM to equilibrium for all grid cells in the study area following the protocol of *Zhuang et al.* [2003], which consisted of using the mean climate from 1901 to 1930, as the equilibrium climate in 1900.

2.5. Albedo Over the Course of Forest Succession

[16] Changes in summer albedo due to changes in the age-class distribution of the ecosystems postfire as calculated in ALFRESCO were computed based on two data sets. One of these, *Amiro et al.* [2006], was based on a synthesis of empirical data from the study region, while the other, *Randerson et al.* [2006] calculated albedo from remotely sensed data from the study region. Changes in albedo due to changes in the snow season were calculated based on *Amiro et al.* [2006]. The two data sets are described in more detail below.

2.5.1. Field-Based Albedo Data Set

[17] *Amiro et al.* [2006] performed a synthesis of field-based albedo measurements across the western boreal zone of North America, taking into account 22 sites in Alaska, Saskatchewan, and Manitoba. Data covered a 150 year chronosequence of forest stands of different ages following natural wildfire, and were collected between 1998 and 2004. These albedo measurements were collected in conjunction with energy balance measurements, including latent heat, sensible heat, ground heat and net radiation. The turbulent flux data were collected using the eddy covariance technique. These data generally represented deciduous broad-leaved species during the early postfire years, with coniferous pine and spruce dominant in the later years.

[18] Based on these data, the summer (June, July, August) albedo is ~0.05 directly following fire, increasing to ~0.13 within the first 10 years postfire, and can be estimated based on the following linear regression equation:.

[19] If stand age $\leq$10 then

$$\text{Summer albedo} = 0.0072 * (\text{stand age}) + 0.0514 \quad (1)$$

$$\left(R^2 = 0.90,\ p < 0.0001\right).$$

[20] At approximately 11 years postfire, the albedo begins to slowly decrease, falling to ~0.07 by age 150, and is calculated based on another linear regression equation:

$$\text{If } 11 \leq \text{stand age} \leq 150 \text{ then}$$

$$\text{Summer albedo} = -0.000396 * (\text{stand age}) + 0.125 \quad (2)$$

$$\left(R^2 = 0.74, p < 0.0001\right).$$

[21] If the stand age following fire is greater than 150 years, a constant value of 0.07 is then assumed.

[22] During the period of snow-covered ground, the albedo can be as high as 0.7 in the recently burned stands with a sparse canopy and a corresponding high reflectance from the snow. By around 25 years of age, the albedo falls to about 0.2 to 0.3 as the forest canopy closes. The albedo over the course of succession during the period of snow-covered ground is fit to an exponential decay regression curve:

$$\text{Winter albedo} = 0.205 + 0.399e^{-0.0561 * \text{stand age}} \quad (3)$$

$$\left(R^2 = 0.66, p < 0.0001\right).$$

2.5.2. Remotely Sensed Albedo Data Set

[23] The remotely sensed summer albedo data set uses Moderate Resolution Imaging Spectroradiometer (MODIS) satellite observations within the burn scars of interior Alaska [*Randerson et al.*, 2006; *Lyons et al.*, 2008]. These data cover forest stands aged between 0 and 55 years following wildfire. These data show that in the first year following fire, summer albedo is approximately 0.10, and continues to increase until it reaches a maximum of ~0.14 25–30 years following fire. After this point, it begins to decline, falling to a value of 0.11 by age 55. These data can be fit to a parabolic function:

[24] If stand age $\leq$55 then

$$\text{Summer albedo} = 0.1099 + (0.0018 * \text{stand age}) - \left(0.00003 * \text{stand age}^2\right) \quad (4)$$
$$\left(R^2 = 0.78, p < 0.0001\right).$$

[25] If the stand age is greater than 55, a constant value of 0.11 is assumed.

[26] The remotely sensed albedo data set during the snow season showed high variability [*Lyons et al.*, 2008] and did not provide a statistically significant fit to a curve. Therefore, for this analysis, we calculate snow season albedo based on just one equation (equation (3), above), while for the summer albedo, we calculate albedo in two ways, based on equations (1) and (2) and based on equation (4). In both summer albedo calculations, we assigned a constant value of 0.19 albedo to the 32,148,300 ha that are considered tundra and did not burn in ALFRESCO simulations. This value of 0.19 is based on measurements of summer albedo collected in Alaskan tundra [*Chambers et al.*, 2005; *Thompson et al.*, 2004].

2.6. Changes in Atmospheric Heating due to Changes in Vegetation and Changes in the Snow Season

[27] We assessed potential changes in atmospheric heating and feedbacks to climate due to changes in both the distribution of postfire ecosystems and changes in the snow season. Based on each set of summer albedo (α) calculations and the estimates of R_{Sin} calculated in TEM, we calculated outgoing shortwave solar radiation (R_{Sout}) as:

$$R_{Sout} = R_{Sin} * \alpha, \text{ for each set of } \alpha. \quad (5)$$

[28] Shortwave net radiation (R_{Snet}) is then calculated as the difference between R_{Sin} and R_{Sout}:

$$R_{Snet} = R_{Sin} - R_{Sout}. \quad (6)$$

[29] Based on the *Amiro et al.* [2006] synthesis of data for the energy fluxes following fire, the summer latent heat (LE) and sensible heat (H) fluxes are normalized to R_{Snet}. From 0 to 10 years of age, LE is about 20% of R_{Snet}, increases to 60% of R_{Snet} at stands 10–25 years of age, and then remains at about 50% of R_{Snet} at stands 25 to 150 years of age. The trajectory of H over the course of succession is largely complementary to that of LE. From 0 to 10 years of age, H is about 60% of R_{Snet}, falling to 30% of R_{Snet} at stands 10–25 years of age, and then increasing to 45% of R_{Snet} at sites 25 to 150 years of age. Following the methodology of *Chapin et al.* [2005] and *Euskirchen et al.* [2007, 2009], seasonal summer atmospheric heating is then computed by multiplying incoming shortwave and longwave radiation by the proportion of incoming shortwave and longwave radiation that is absorbed by the land surface times the proportion of net shortwave and longwave radiation that is transferred to the atmosphere:

$$\{RSin + RLin\} \times \{\frac{RSnet + RLnet}{RSin + RLin}\} \times \{\frac{H + LE}{RSnet + RLnet}\}. \quad (7)$$

[30] Note that the ratios in this calculation are key, in that the terms described collapse into H + LE, but we have used the ratios to derive H + LE.

[31] We estimated changes in atmospheric heating due to changes in the length of the snow season, in terms of both snowmelt in the spring and snow return in the fall. Our estimates of changes in heating due to changes in snow cover follow the methodology outlined by *Euskirchen et al.* [2007, 2009]. We use TEM-derived values of R_{Sin} and literature-derived values of heat fluxes, with the literature-derived values of the heat fluxes being the same as those in Table 1 of *Euskirchen et al.* [2007] for the tundra, boreal evergreen needleleaf forest, and boreal deciduous forest. As above, we multiply incoming shortwave and longwave radiation by the proportion of incoming shortwave and longwave radiation that is absorbed by the land surface times the proportion of net shortwave and longwave radiation that is transferred to the atmosphere (equation (7)). We then compare presnowmelt and postsnowmelt and presnow and postsnow return energy budgets to estimate the changes in snowmelt and snow return on atmospheric heating: {[Daily atmospheric heating postsnowmelt (*or presnow return*)] – [Daily atmospheric heating presnowmelt (*or postsnow return*)] **x** [Change in snow cover duration]}, where the daily atmospheric heating is in units of MJ m^{-2} d^{-1} and the change in snow cover duration is in days $year^{-1}$. The estimates of heating are then averaged over the length of the snow-free season, as calculated in the water balance model. The changes in atmospheric heating due to the change in the snow-free season are computed based on a constant forest stand age distribution (that in 2003) and also using the dynamic forest stand age distribution from 2003 to 2100 based on the ALFRESCO simulations. Estimates of both summer and winter heating are presented at the decadal timescale in W m^{-2} based on the mean annual changes in the surface energy flux.

2.7. Climate Data

[32] We chose two future climate scenarios described by *Nakićenović and Swart* [2000] and two of the modeled global climate model (GCM) outputs for use as input climate data. The scenarios we chose were the A2 and B2. The A2 scenario exhibits greater accumulated radiative forcing and a faster rate of warming than the B2 scenario [*Intergovernmental Panel on Climate Change* (*IPCC*), 2000; *Nakićenović and Swart*, 2000]. We chose two GCMs (Hadley CM3, and PCM) that represented a range of sensitivity to greenhouse gas forcing.

[33] We followed the same procedure as described by *Euskirchen et al.* [2009] to process these climate data. We downloaded the monthly data for air temperature, precipi-

tation, and cloudiness from the IPCC Data Distribution Center (http://www.ipcc-data.org/). Since the outputs from the GCMs are not matched directly to historical climate, we matched the projections to the historical climate record to ensure that there was continuity in the time series using baseline observational data. We overlaid the projected changes in climate on the mean historical climate based on the period 1961–1990 using the database of historical climate obtained from the Climate Research Unit, which includes precipitation, air temperature, and cloudiness data for the years 1901–2002 (CRU [*New et al.*, 2002; *Mitchell and Jones*, 2005]). The absolute differences in mean monthly temperatures and the ratios in monthly precipitation and monthly mean cloudiness for 1961–1990 were then calculated, with the baseline values corresponding to the simulated climate from the GCMs.

[34] Since this procedure resulted in "smooth curves" of changes in temperature, cloudiness, and precipitation for the future scenarios, we then added interannual variability to the future climate. We did this by randomly picking a sequence of years within the 1901–2002 CRU period, using the same seed for all half -degree grid cells so each cell used the same sequence of years. We calculated the mean value for the CRU period for each of the grid cells, and then computed scenario change for each GCM scenario as: (GCM scenario value for location)/(mean value for location). Finally, the forecasted value for each grid cell was calculated as (value from random base year)*(scenario change). The modeling results from the "smoothed data" and those with interannual variability added both show the same amount of change for all three of the climate variables, air temperature, precipitation, and cloudiness, by the end of 2100 [see also *Euskirchen et al.*, 2009].

[35] Since the ALFRESCO models was run at a 1 km by 1 km spatial resolution to simulate the interactions between fire and vegetation heterogeneity across the region, we used a simple resampling algorithm to process each data set and generate climate data for a grid of 1 km by 1 km pixels, as described by *Rupp et al.* [2007]. The data sets were first converted to the Northern Hemisphere 25 km by 25 km Equal-Area Scalable Earth (EASE) grid [*Drobot et al.*, 2006]. The 625 1 km by 1 km pixels within an EASE pixel were then populated with the climate data of the EASE pixel.

[36] The mean annual air temperature between 2003–2100 over the domain increased significantly ($p < 0.0001$) in all scenarios with a maximum change of approximately $+0.10°C\ yr^{-1}$ in the A2 Hadley CM3 climate and a minimum change of approximately $+0.04°C\ yr^{-1}$ in the B2 PCM climate (Figure 2a). Across all climates, air temperature increases were generally greater in the winter (December, January, February; DJF) than in other seasons. Precipitation also significantly ($p < 0.0001$) increased across all climates, with the greatest increase ($\sim$1.0 mm yr^{-1}) occurring in the B2 HadCM3 climate, and the smallest increase (0.5 mm yr^{-1}) occurring in the B2 PCM climate (Figure 2b). Cloudiness increased under all scenarios except for the B2 PCM during the fall (September, October, November; SON) and during the winter for the A2 PCM and B2 PCM climates. However, these changes in cloudiness were only statistically significant during the spring (March, April, May; MAM) in the A2 and B2 Hadley CM3 climates and for all climates in the summer (June, July, August; JJA). Incoming solar radiation, as calculated in the Terrestrial Ecosystem Model based on the cloudiness data (see section 2.4 above) only showed significant ($p < 0.0001$) changes in the summer (JJA), when it decreased from between -0.025 W m^{-2} yr^{-1} in the B2 PCM climate to -0.065 W m^{-2} yr^{-1} in the A2 Hadley CM3 climate due to increases in cloudiness.

3. Results

3.1. Changes in Landscape Age Structure due to Changes in the Fire Regime

[37] Across all climate scenarios, the amount of area burned increased until the decade between 2061–2070, after which it generally began to decline (Figure 3). During this decade between 2061–2070, the area burned ranged from a mean of 4,621,100 ha yr^{-1} for the B2 PCM climate (Figure 3d) to a maximum of 5,765,400 ha yr^{-1} in the A2 Hadley CM3 climate (Figure 3a). Coinciding with the increase in the amount of area burned, the landscape showed a trend toward an increase in younger forests due to fire disturbance between the years 2003–2100 (Figure 4). Forests aged between 20–40 years of age increased the most based on the slopes of least squares linear regression (21,219–22,588 ha yr^{-1}; Figures 4c and 4d). However, postfire ecosystems between 0 to 20 years of age increased almost as much as those between 20–40 years (19,861–19,918 ha yr^{-1}; Figures 4c and 4d). Forests 80 or more years of age exhibited a large decrease based on the slopes of least squares linear regression ($-134{,}492$ ha yr^{-1}; Figure 4h).

3.2. Changes in the Snow Season

[38] Across the climate scenarios, changes in snowmelt ranged from 1.3 to 3.2 d $decade^{-1}$ earlier (Table 1) and changes in snow return were similar, ranging from 1.3 to 3.0 d $decade^{-1}$ later, with the strongest trends occurring under the warmer climate scenarios (e.g., A2 Hadley CM3; A2 PCM; Figure 2a). Averaged across all climates, the snow season was approximately 4.5 d $decade^{-1}$ shorter. By year 2100, the mean number of snow-free days across the region was $\sim$ 200, which was $\sim$45 more snow-free days compared to the beginning of the simulation in 2003 (Table 1).

3.3. Changes in Albedo

[39] Our estimates of changes in summer albedo based on equations (1) and (2) indicated that between 2003–2100 the landscape experienced increases in summer albedo due to increases in early and midsuccessional ecosystems following fire (Figure 5a). The mean change in albedo was from 0.140 in 2003 to 0.155 in 2100, with the maximum change in albedo occurring under the A2 Hadley CM3 climate (0.140 in 2003 to 0.160 in 2100), and the minimum change in albedo occurred in the B2 PCM climate (0.140 in 2003 to 0.150 in 2100).

[40] Estimates of changes in summer albedo based on the remotely sensed estimates of albedo represented by equation (4) were much smaller than those based on equations (1) and (2). The mean change was from 0.175 in 2003 to 0.181 in 2100 (Figure 5b). The effects of the changes in distribution of ecosystems postfire on albedo are small because there were increases in both the youngest ages (0 to 20 year) of ecosystem postfire when albedo is low

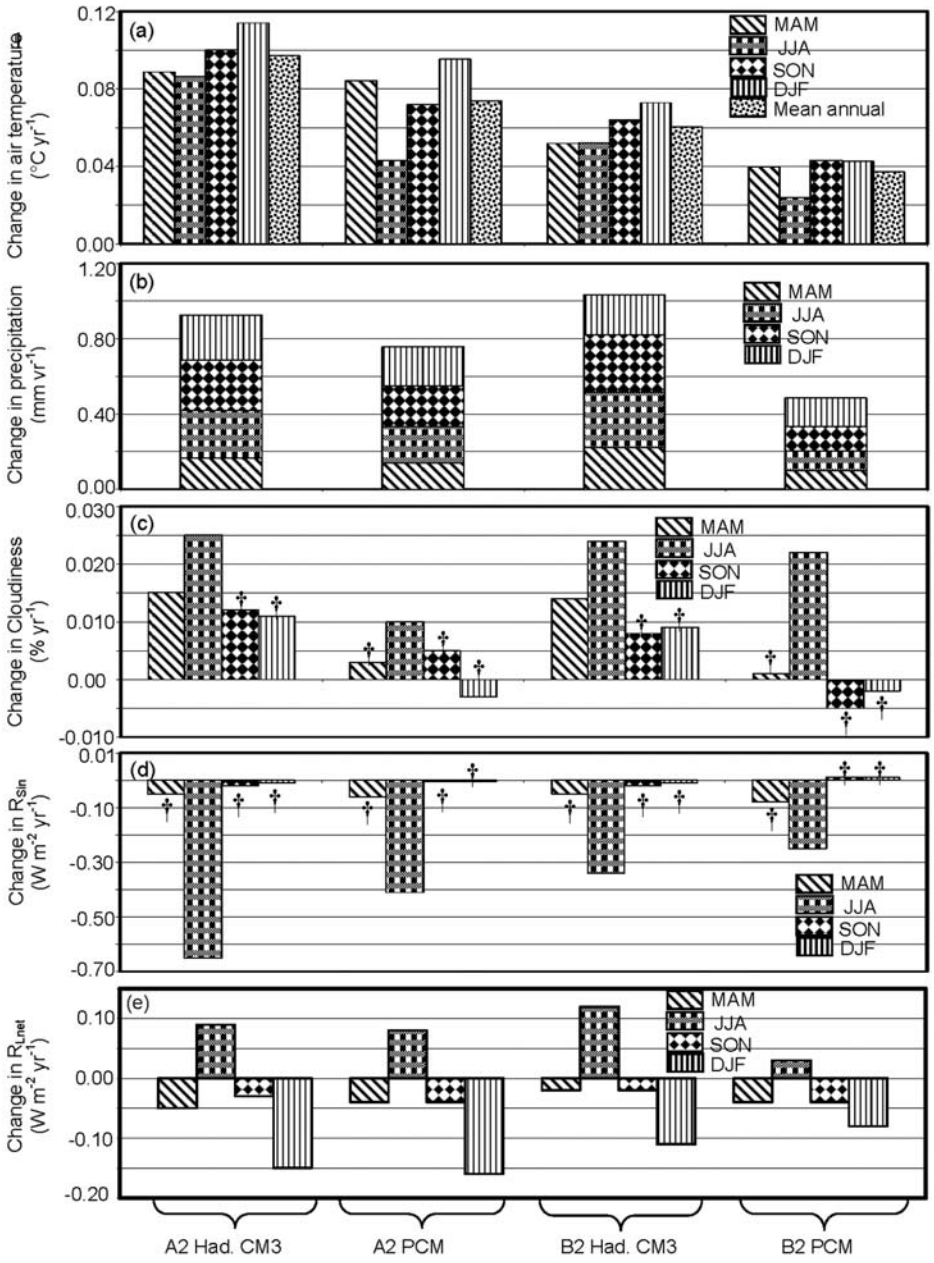

Figure 2. Trends in (a) air temperature, (b) precipitation, (c) cloudiness, (d) incoming shortwave solar radiation (R_{Sin}), and (e) net longwave radiation (R_{Lnet}) in the western Arctic between 2003 and 2100 based on two climate models and scenarios. Trends are based on the slopes of least squares linear regression. All trends in air temperature, precipitation, and R_{Lnet} were statistically significant at $p < 0.0001$. For cloudiness and R_{Sin}, trends marked with daggers were not statistically significant at $p < 0.0001$. MAM, March, April, and May; JJA, June, July, and August; SON, September, October, and November; DJF, December, January, and February; Mean is the mean across all scenarios and climate models.

and the intermediate-aged (20–40 years) when albedo is high (equation (4)).

[41] During the period of snow covered ground, albedo, based on equation (3), showed a greater change than summer albedo, increasing by ~0.05 between 2003–2100 (Figure 5c). An increase in forests in the 20–80 year age category toward the end of the 21st century (Figures 4d and 4e) caused a decrease in the snow season albedo at the end of the simulation compared to 20–30 years earlier. This is because snow season albedo decreases in sites greater than 20 years. However, with the increase in the 0 to 20 year stands, and the decrease in stands >80, the snow season albedo remained greater in 2100 than 2003.

3.4. Changes in Atmospheric Heating

[42] Changes in atmospheric heating based on the calculations described in equation (7) were due more to the shortening of the snow season than to changes in the forest

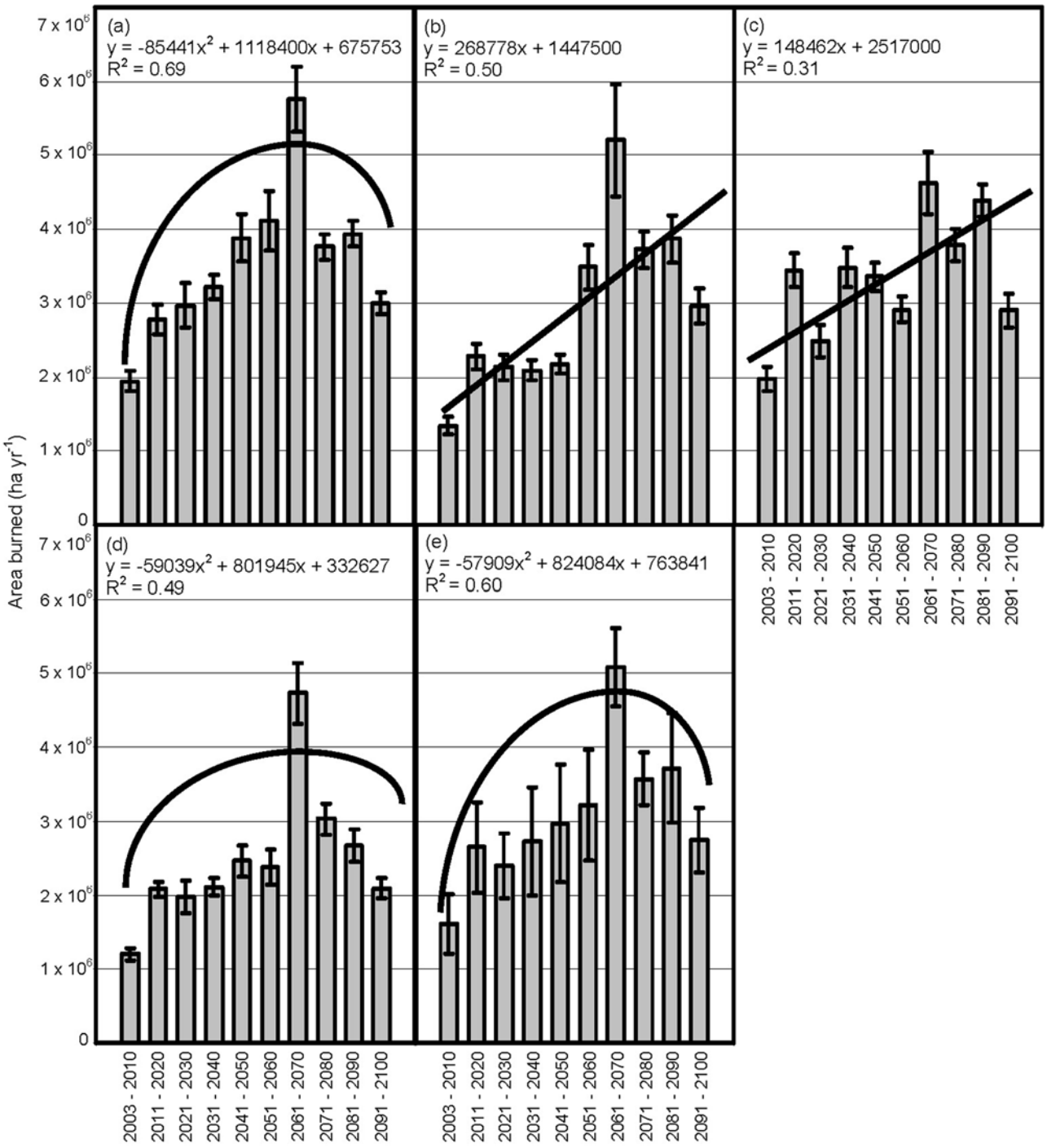

Figure 3. Mean (standard deviation) area burned per year by decade and climate scenario between 2001 and 2100. (a) A2 Hadley CM3; (b) A2 PCM; (c) B2 Hadley CM3; (d) B2 PCM; (e) means across all scenarios in Figures 3a–3d. A parabolic or least squares regression line is fit to the means of the data, with $p < 0.0001$ for all regressions in Figures 3a–3e.

stand age distribution across the landscape under future fire regimes (Figure 6). Figure 6 shows two sets of changes in summer atmospheric heating estimates since, as described in section 2.6, we incorporated two sets of albedo estimates (the remotely sensed and empirical) in our calculations of atmospheric heating in equation (7). The summer atmospheric heating acted as a negative feedback of -0.9 ± 0.2 W m^{-2} $decade^{-1}$, with no significant difference ($p > 0.05$) between the estimates of atmospheric heating that take into account the empirical albedo estimates based on equations (1) and (2) versus the estimates of atmospheric heating that take into account albedo based on remotely sensed estimates equation (4) (Figure 6a). Changes in atmospheric heating due to changes in the snow season

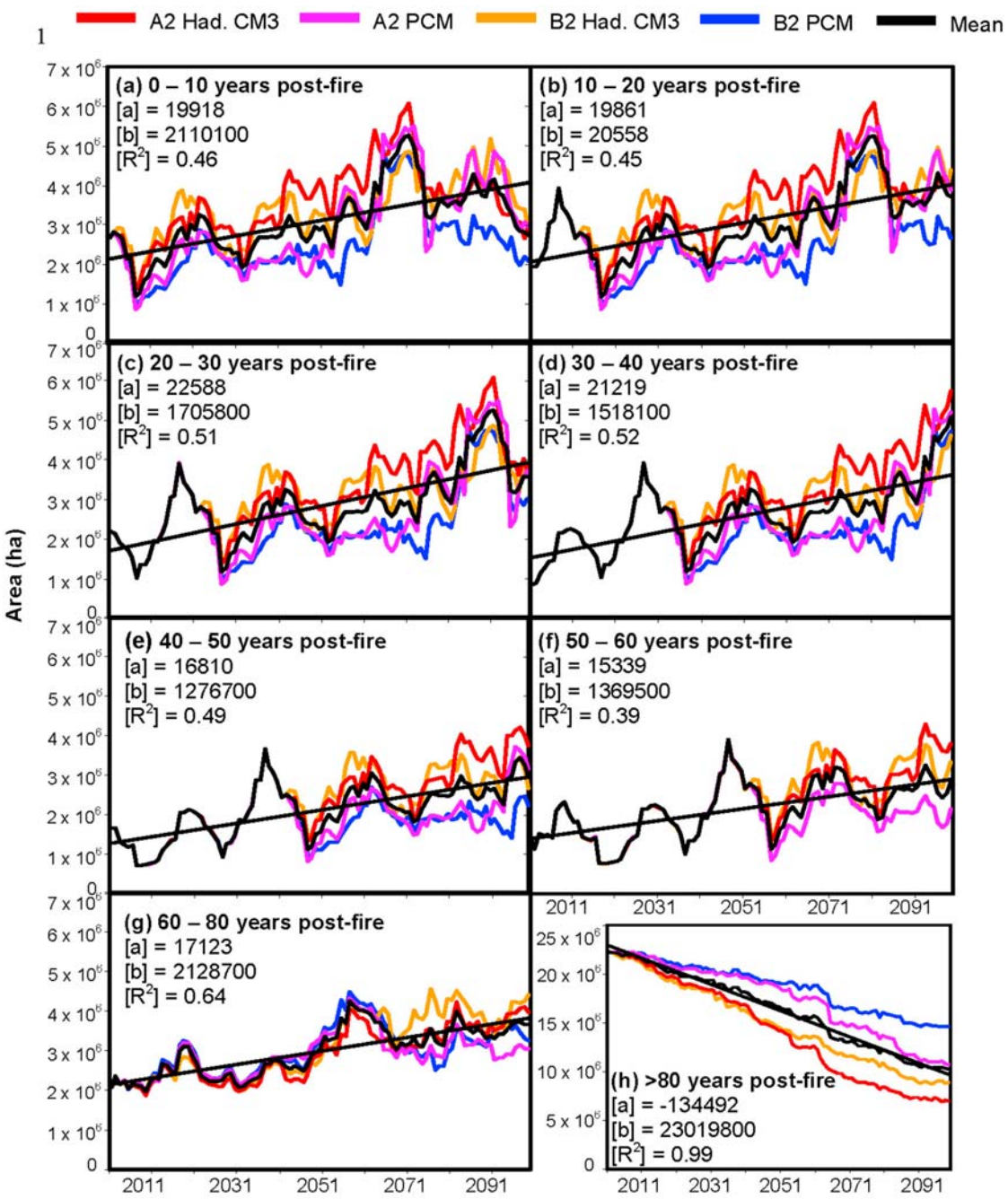

Figure 4. Changes in the distribution of the age of the ecosystems postfire based on ALFRESCO simulations. A least squares regression line is fit to the means of the data, with $p < 0.0001$ for all regressions in Figures 4a–4c. [a] is slope, and [b] is intercept.

acted as a positive feedback of +4.8 ± 1.7 W m^{-2} $decade^{-1}$ if the forest stand age distribution from the year 2003 was held constant, and +4.3 ± 1.5 W m^{-2} $decade^{-1}$ if the dynamic forest stand age distribution based on the ALFRESCO simulations for 2003–2100 was incorporated (Figure 6b). Changes in the atmospheric heating of snow covered and snow-free ground were greater in spring than in autumn (Figure 6b). For example, the decrease in snow cover duration due to changes in the timing of snowmelt was a mean of 2.3 days earlier $year^{-1}$ and 2.2 days later $year^{-1}$ due to changes in the timing of snow return (Table 1), but there was a disproportional increase in heating due to the timing of snowmelt (3.8 ± 1.4 W m^{-2} $decade^{-1}$) compared to the timing of snow return (1.0 ± 0.3 W m^{-2} $decade^{-1}$; Figure 6). This is due to the asymmetry of snowmelt and snow return over the region. That is, snowmelt primarily occurs between the vernal equinox and the summer solstice while snow return generally occurs between the autumn equinox and winter solstice. The greater amount of solar input at the time of snowmelt is primarily responsible for greater snow cover–climate feedback in the spring [see also *Euskirchen et al.*, 2007]. Adding the negative effect of changes in summer atmospheric heating to the positive effect of changes in snow season atmospheric

Table 1. Changes in the Period of Snow-Covered Ground Between the Years 2003 and 2100 for Each Climate Scenario[a]

Climate Scenario	Change (d decade^{-1})			Length of Snow-Free Season (days) at 2100
	Snowmelt	Snow Return	Melt Plus Return	
A2 Hadley CM3	−3.0	3.0	6.0	218
A2 PCM	−3.2	2.3	5.5	209
B2 Hadley CM3	−1.8	2.0	3.8	196
B2 PCM	−1.3	1.3	2.6	177
Mean	−2.3	2.2	4.5	200

[a]A negative value of snowmelt indicates an earlier trend, and a positive value for snow return indicates a later trend. For the total (melt plus return), a positive value indicates a shorter snow season.

heating resulted in an increase in atmospheric heating ranging from a maximum of ~3.9 W m^{-2} decade^{-1} (assuming constant forest stand age distributions; Figure 6c) to minimum of ~3.4 W m^{-2} decade^{-1} (incorporating the dynamic forest stand age distributions; Figure 6d).

[43] We assessed the change in atmospheric heating from changes in the forest stand age distributions across the region under future fire regimes and from changes in the snow season (W m^{-2}, anomaly) per change in climate variables, including air temperature precipitation, summer R_{Sin}, by performing least squares linear regression analyses for each climate scenario (Table 2). Changes in summer atmospheric heating were most sensitive to changes in summer R_{Sin} ($p < 0.0001$ across all climates; Table 2), but were also sensitive ($p < 0.05$) to changes in summer precipitation and mean annual temperature under some climate scenarios. Changes in snowmelt and snow return were highly sensitive to changes in mean annual temperature across all climates ($p < 0.0001$ across all climates; Table 2), but not significantly sensitive ($p > 0.05$) to changes in precipitation or R_{Sin}. Overall, these analyses illustrate the importance of changes in summer R_{Sin} to changes in summer atmospheric heating, and to changes in air temperature on snow season atmospheric heating.

4. Discussion

4.1. Overview

[44] This study evaluated climate feedbacks due to future land cover changes caused by both changes in fire regimes and snow cover during the years 2003–2100. Our study supports the conclusion that increased atmospheric heating due to decreases in snow cover was approximately four times larger than the decreased atmospheric heating due to changes in land cover under future fire regimes. In the discussion below, we evaluate (1) the parameterizations and model simulations as they pertain to the results of this study, (2) the potential importance of burn severity, and (3) other forcing agents that we did not consider in this study, but are important to examine in order to gain a better understanding of climate feedbacks in this region.

4.2. Evaluation of Parameterizations and Model Simulations

4.2.1. Albedo Parameterizations and Changes in Cloudiness

[45] The two summer albedo functions based on the field collected data (equations (1) and (2)) versus the remotely sensed collected data (equation (4)) show general qualitative agreements but are quantitatively different. They both show a general increase in albedo postfire, and a decline in the later successional forests. However, the timing of this decline differs. In the field collected data, albedo increases until approximately year 10, and then declines thereafter, while in the remotely sensed collected data, the albedo

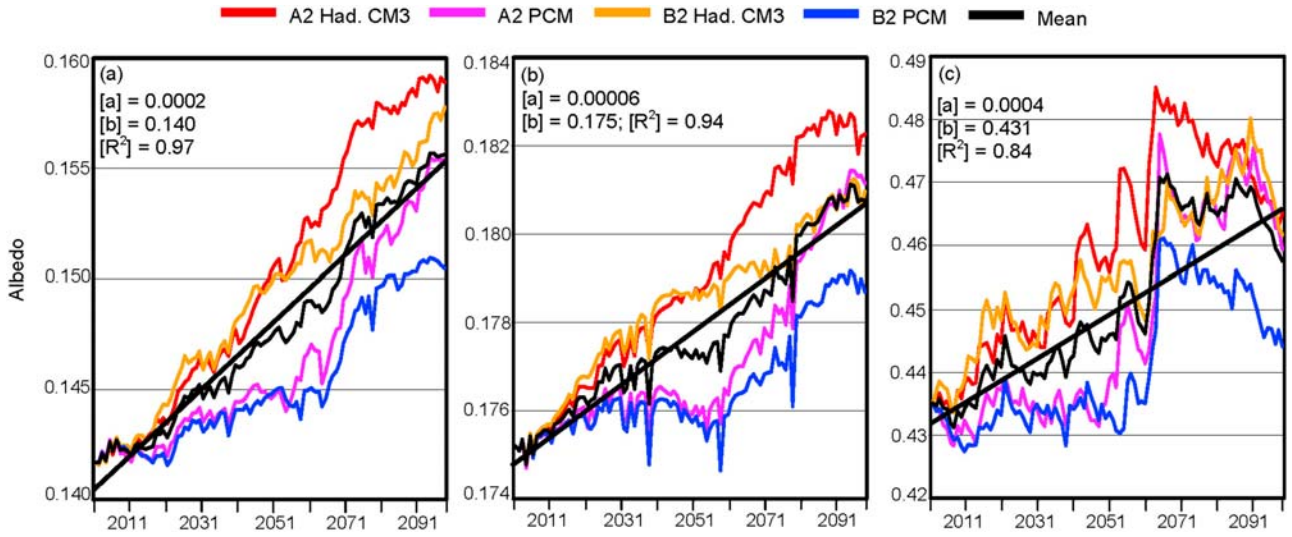

Figure 5. Changes in albedo due to the changes in the postfire distributions of the ecosystems over the study region for the years 2003–2100. (a) These changes are based on *Amiro et al.* [2006] equations for summer albedo. (b) These changes are based on *Randerson et al.* [2006] and *Lyons et al.* [2008] equations for summer albedo. (c) These changes are based on *Amiro et al.* [2006] equations for snow season albedo. A least squares regression line is fit to the means of the data, with $p < 0.0001$ for all regressions in Figures 5a–5c. [a] is slope, and [b] is intercept.

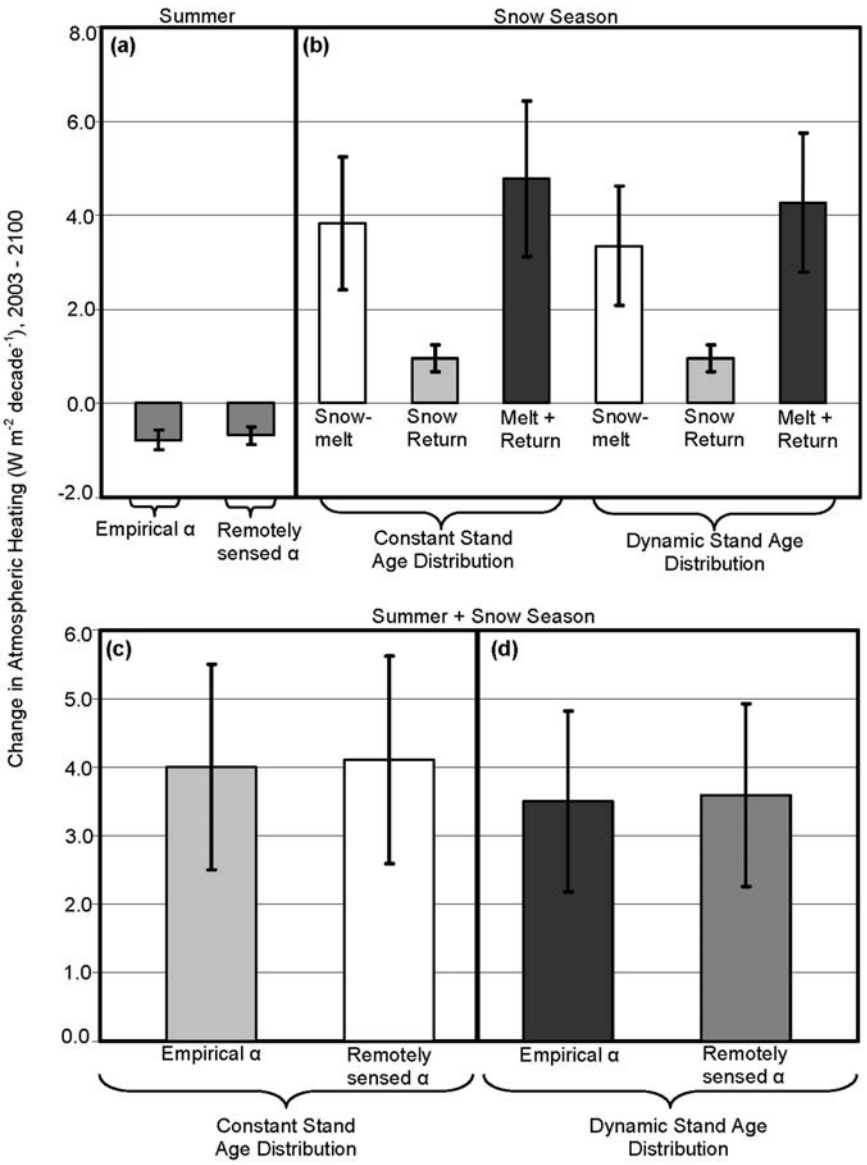

Figure 6. Mean changes in atmospheric heating from 2003 to 2100 across all four input climate scenarios (W m^2 $decade^{-1}$, ± standard deviation). (a) The changes in atmospheric heating are due to summer albedo change based on both empirical and remotely sensed estimates of albedo (α). (b) The changes in atmospheric heating are due to the snow season albedo changes, taking into account both a constant forest stand age distribution and a dynamic forest stand age distribution. (c) The changes in atmospheric heating for the summer and snow season are summed and are based on the constant forest stand age distribution for the snow season. (d) The changes in atmospheric heating for the summer and snow season are summed and incorporate the dynamic stand age distributions for the snow season.

peaks at 25–30 years postfire and declines thereafter. Furthermore, the values of albedo differ between the two data sets, ranging from ~0.05 to ~0.12 in functions based on the field-collected data set (equations (1) and (2)) to ~0.11 to ~0.14 in the function based on the remotely sensed data (equation (4)). Since both data sets calculated albedo based on the daily totals (e.g., the ratio of total reflected to total incoming solar radiation), these differences may be attributed to a combination of scaling and remote sensing issues associated with satellite retrievals [*Lyons et al.*, 2008].

[46] Even though these two albedo functions yielded different estimates of changes in summer albedo between 2003–2100 (Figures 5a and 5b), this difference ultimately had little impact on the estimate of atmospheric heating (Figure 6b). Changes in the summer atmospheric heating were ultimately most sensitive to the decrease in R_{Sin}, which followed from the increase in summer cloudiness (Figures 2c and 2d). Longwave radiation also increased in the summer under the increases in cloudiness (Figure 2e), although the changes in atmospheric heating were only sensitive to this change under two climate scenarios (Table 2). While clouds in global climate models are one

Table 2. Change in Summer Atmospheric Heating per Change in Mean Annual Temperature, Summer Incoming Solar Radiation R_{Sin}, and Summer Precipitation, and Change in Snow Season Atmospheric Heating per Change in Mean Annual Temperature[a]

Variable	Climate	Change in Anomaly of Mean Annual Air Temperature (W m^{-2} per °C)	Change in Anomaly of JJA R_{Sin} (W m^{-2} per W m^{-2})	Change in Anomaly of JJA R_{Lnet} (W m^{-2} per W m^{-2})	Change in Anomaly of JJA Precipitation (W m^{-2} per mm)
Summer	A2 Had. CM3	−0.93	25.71	−0.57	−0.103
atmospheric		(0.12; 0.0004)	(0.94; < 0.0001)	(0.10; 0.02)	(0.11; 0.005)
heating with	A2 PCM	−0.25	25.14	ns	−0.08
empirical		(0.94; < 0.0001)	(0.94; < 0.0001)		(0.10; 0.005)
albedo	B2 Had. CM3	ns	24.88	ns	−0.08
estimates			(0.95; < 0.0001)		(0.11; 0.0006)
	B2 PCM	ns	24.55	ns	ns
			(0.97; < 0.0001)		
	mean	ns	25.03	ns	−0.08
			(0.95; < 0.0001)		(0.10; 0.005)
Summer	A2 Had. CM3	−0.80	24.37	−0.48	−0.09
atmospheric		(0.10; 0.001)	(0.95; < 0.0001)	(0.10; 0.03)	(0.11; 0.001)
heating with	A2 PCM	−0.23	23.99	ns	−0.07
remotely		(0.94; < 0.0001)	(0.95; < 0.0001)		(0.07; 0.008)
sensed albedo	B2 Had. CM3	ns	23.68	ns	−0.07
estimates			(0.96; < 00001)		(0.10; 0.0015)
	B2 PCM	ns	23.45	ns	ns
			(0.97; < 0.001)		
	mean	ns	23.84	ns	−0.07
			(0.96; < 0.0001)		(0.07; 0.008)

Variable	Climate	Time of Snow Change	Change in Anomaly of Mean Annual Air Temperature (W m^{-2} per °C)
Snow season	A2 Had. CM3	melt	0.14 (0.66; < 0.0001)
atmospheric		return	0.04 (0.79; < 0.0001)
heating	A2 PCM	melt	0.16 (0.59; < 0.0001)
		return	0.06 (0.69; < 0.0001)
	B2 Had. CM3	melt	0.15 (0.49; < 0.0001)
		return	0.05 (0.67; < 0.0001)
	B2 PCM	melt	0.09 (0.40; < 0.0001)
		return	0.03 (0.54; < 0.0001)
	Mean	melt	0.17 (0.57; < 0.0001)
		Return	0.05 (0.70; < 0.0001)

[a]JJA, June, July, August. Analyses are based on coefficients obtained from least squares linear regression. Numbers in parenthesis represent R^2 and p values, respectively, and ns indicates not statistically significant ($p > 0.05$).

of the biggest uncertainty in future projections of the Arctic climate [*Curry et al.*, 1996], across all the climates presented here there was agreement across the GCMs and scenarios that summer cloudiness will increase. This trend is also seen in other studies which have shown a statistically significant increase in summer cloudiness during the last several decades of the twentieth century [*Wang and Key*, 2003, 2005]. A decrease or no change in the summer cloudiness, resulting in a decrease or no change in R_{Sin}, would have a large influence on the estimates of changes in atmospheric heating associated with the changes in forest stand age simulated in this study. Likewise, a significant increase in cloudiness resulting in an increase in R_{Sin} during the time of snowmelt and snow return may also influence the results of changes in atmospheric heating due to changes in the snow season presented here.

4.2.2. ALFRESCO Simulations

[47] The approach presented in this study benefits from the incorporation of a relatively fine-scale representation (1 km by 1 km) of vegetation disturbance and area burned. *Rupp et al.* [2007] found that ALFRESCO was able to provide reasonable estimates of area burned when driven by the historical CRU data set compared to other driving historical climate data sets. These other climate data sets included those from the National Centers for Environmental Prediction–National Center for Atmospheric Research (NCEP-NCAR) reanalysis product [*Kistler et al.*, 2001], and the data set based on the fifth-generation Pennsylvania State University–NCAR Mesoscale Model (MM5 [*Wu et al.*, 2007]). The main reason that ALFRESCO provided the most reasonable estimates when driven with the CRU data set is associated with differences in precipitation among the climates [*Rupp et al.*, 2007]; both the NCEP1 and MM5 data sets produced very little area burned historically because of substantially colder and wetter growing seasons than those based on the CRU data. Since we matched the projected climates to the historical climate record based on the CRU data (see section 2.7), a technique recommended by *Rupp et al.* [2007], we have some confidence that the ALFRESCO projections of area burned are reasonable. Furthermore, the estimates of area burned presented here generally agree with those presented in the study of *Balshi et al.* [2008], which used a Multivariate Adaptive Regression Splines (MARS) approach in conjunction with future climate data sets to estimate area burned within the same study region.

4.3. Burn Severity

[48] Burn severity, the proportion of soil organic matter and tree material consumed, is a critical variable regulating landscape patterns of postfire succession [*Johnstone and Kasischke*, 2005; *Johnstone and Chapin*, 2006], and burn severity is expected to be greater under increases in temperature [*Stocks et al.*, 2000; *Amiro et al.*, 2006]. Neither the simulations with the version of the ALFRESCO model presented here, nor the estimates of postfire albedo, took burn severity into account. However, the inclusion of this parameter in future work may serve to complement the analysis presented here. For example, stands with a higher burn severity might exhibit greater exposure of snow due to greater vegetation consumption and due to increased toppling of trees when the soil organic matter in which they are rooted is consumed compared to stands with lower exposure. Therefore, future estimates of albedo over the course of postfire succession may be more accurate if a metric of burn severity is incorporated [*Lyons et al.*, 2008].

[49] Furthermore, increases in burn severity have been linked to regrowth patterns that favor a higher deciduous component over the course of succession [*Kasischke and Johnstone*, 2005]. This would lead to a longer period of higher summer albedo values compared to low-severity burns where conifers become dominant earlier in succession. Consequently, more severe fires in the future may lead to a stronger negative feedback to atmospheric heating.

4.4. Other Forcing Agents

[50] There are other forcing agents in the western Arctic that we did not consider in this study. A comprehensive analysis of the climate forcings of boreal fires found that averaged over an 80 year fire cycle, the negative forcing from surface albedo is greater than the smaller, positive biogeochemical forcing, with a net effect of -2.3 ± 2.2 W m^{-2} [*Randerson et al.*, 2006]. However, in the first year following fire, positive biogeochemical forcing from greenhouse gas emission, ozone, black carbon deposited on snow and ice, and aerosols exceeds the negative albedo forcing. Other studies have similarly found that in boreal forests the biophysical effects of deforestation promote more cooling than those associated with increased carbon uptake due to afforestation [*Betts*, 2000; *Bala et al.*, 2007]. Increased disturbance from insect outbreaks will also shift the forest to a younger age class [*Boucher and Mead*, 2006; *Kurz et al.*, 2008] increasing the surface albedo, possibly leading to a negative feedback on atmospheric heating. Trees may expand into the tundra, decreasing surface albedo, leading to positive feedback on atmospheric heating. However, previous analyses suggest that northward tree migration into our study region would likely take centuries to occur [*Chapin and Starfield*, 1997; *Rupp et al.*, 2001]. Nevertheless, it is important to note that if northward tree migration in Alaska were substantial in the 21st century, then summer atmospheric heating would be substantially larger, but it might make these regions less sensitive to changes in snow cover duration.

[51] An increase in the shrubiness of the tundra may also promote a positive feedback to atmospheric heating, although this might be small. In a synthesis of field data from northern Alaska, *Chapin et al.* [2005] found that past increases in northern Alaska vegetation from 1950 to present accounted for an increase in atmospheric heating of $\sim$0.20 W m^{-2} $decade^{-1}$, while the increase in atmospheric heating due to snowmelt advance accounted for $\sim$3.3 W m^{-2} $decade^{-1}$. In the future, under a complete conversion to shrubland or forest, the increase in summer atmospheric heating was estimated as $\sim$6.4 W m^{-2} due to shrubland conversion and 24.5 W m^{-2} due to forest conversion, with a smaller increase under the effect of snowmelt advance, 2.5 W m^{-2} $decade^{-1}$ in the tundra, and $\sim$1.4 W m^{-2} $decade^{-1}$ in the forest [*Chapin et al.*, 2005]. Recent work building on the study of *Chapin et al.* [2005] provides a transient analysis of how changes in vegetation and snow cover of northern Alaska are likely to influence atmospheric heating during the 21st century [*Euskirchen et al.*, 2009]. This analysis finds that an increase of shrub tundra in northern Alaska would increase regional summer heat absorption by 0.34 ± 0.23 W m^{-2} $decade^{-1}$ during the 21st century, while the changes in snow cover would be similar to (3.3 ± 1.24 W m^{-2} $decade^{-1}$) that of *Chapin et al.* [2005]. That is, this analysis suggests that the degree of conversion to shrubland in the 21st century would only affect summer atmospheric heating approximately 5% of the complete conversion to shrubland [*Euskirchen et al.*, 2009]. An earlier snowmelt would likely cause an earlier green-up of the deciduous species that may decrease fire hazard, but this interaction was not included in this analysis. While all these factors warrant careful consideration in studies of climate feedbacks in this region, it is important to note that they may not all occur in concert or linearly. That is, increases in the biomass of an aggrading forest may occur over a relatively long period of time while increases in albedo may occur rapidly after timber harvest or fire [*Betts*, 2000].

5. Conclusion

[52] An ongoing challenge to the global-change modeling community is to understand how changes in the land surface impact atmospheric heating. Here, we examined two of these land surface changes in the western Arctic: (1) changes in the distribution of forest age under changes in fire regimes, and (2) changes in the land surface due to changes in the timing of snowmelt and snow return. We found that between 2003–2100 changes in the fire regime that resulted in a larger proportion of early successional ecosystems across the landscape had a negative feedback of 0.9 W m^{-2} $decade^{-1}$ on atmospheric heating. Decreases in the duration of the snow season increased atmospheric heating by 4.3 W m^{-2} when the dynamic forest stand age distributions from the changes in the fire regime were taken into account. This resulted in an overall increase in atmospheric heating of 3.4 W m^{-2} $decade^{-1}$. Considering these terrestrial feedbacks to atmospheric heating in concert with those from a diminishing sea ice [*Perovich et al.*, 2007], suggests amplification of atmospheric heating due to changes in the Arctic.

[53] **Acknowledgments.** This work was supported by the National Science Foundation Arctic System Science Program as part of the Western Arctic Linkage Experiment and Fire Mediated Changes in the Arctic Project (OPP-095024 and OPP-0328282). Funding was also provided by the NSF for the Arctic Biota/Vegetation portion of the "Climate of the Arctic: Modeling and Processes" project (OPP-0327664). Mark Olson assisted

with data set processing. We thank two anonymous reviewers for their helpful comments on an earlier version of this manuscript.

References

Amiro, B. D., et al. (2006), The effect of post fire stand age on the boreal forest energy balance, *Agric. For. Meteorol.*, *140*, 41–50, doi:10.1016/j.agrformet.2006.02.014.

Bala, G., K. Caldeira, M. Wickett, T. J. Phillips, D. B. Lobell, C. Delire, and A. Mirin (2007), Combined climate and carbon-cycle effects of large-scale deforestation, *Proc. Natl. Acad. Sci. U. S. A.*, *104*, 6550–6555, doi:10.1073/pnas.0608998104.

Baldocchi, D., F. M. Kelliher, T. A. Black, and P. G. Jarvis (2000), Climate and vegetation controls on boreal zone energy exchange, *Global Change Biol.*, *6*(S1), 69–83, doi:10.1046/j.1365-2486.2000.06014.x.

Balshi, M. S., A. D. McGuire, P. Duffy, M. Flannigan, J. Walsh, and J. Melillo (2008), Assessing the response of area burned to changing climate in western boreal North America using a Multivariate Adaptive Regression Splines (MARS) approach, *Global Change Biol.*, *14*, 1–23.

Betts, R. A. (2000), Offset of the potential carbon sink from boreal forestation by decreases in surface albedo, *Nature*, *408*, 187–190, doi:10.1038/35041545.

Boucher, T. V., and B. R. Mead (2006), Vegetation change and forest regeneration on the Kenai Peninsula, Alaska following a spruce beetle outbreak, 1987–2000, *For, Ecol. Manage.*, *227*, 233–246, doi:10.1016/j.foreco.2006.02.051.

Calef, M. P., A. D. McGuire, and F. S. Chapin III (2008), Human influences on wildfire in Alaska from 1988 through 2004: An analysis of spatial patterns of human impacts, *Earth Interact.*, *12*, 1–17, doi:10.1175/2007EI220.1.

Chambers, S. D., J. Beringer, J. T. Randerson, and F. S. Chapin III (2005), Fire effects on net radiation and energy partitioning: Contrasting responses of tundra and boreal forest ecosystems, *J. Geophys. Res.*, *110*, D09106, doi:10.1029/2004JD005299.

Chang, J.-H. (1968), *Climate and Agriculture: An Ecological Survey*, Aldine, Chicago, Illinois.

Chapin, F. S., III, and A. M. Starfield (1997), Time lags and novel ecosystems in response to transient climatic change in arctic Alaska, *Clim. Change*, *35*, 449–461, doi:10.1023/A:1005337705025.

Chapin, F. S., III, T. S. Rupp, A. M. Starfield, L. DeWilde, E. S. Zavaleta, N. Fresco, J. Henkelman, and A. D. McGuire (2003), Planning for resilience: Modeling changes in human-fire interactions in the Alaskan boreal forest, *Front. Ecol. Environ*, *1*, 255–261, doi:10.1890/1540-9295(2003)001[0255:PFRMCI]2.0.CO;2.

Chapin, F. S., III, et al. (2005), Role of land-surface changes in arctic summer warming, *Science*, *310*, 657–660, doi:10.1126/science.1117368.

Christensen, J. H., et al. (2007), Regional climate projections, in *Climate Change 2007: The Physical Science Basis. Contribution of Working Group I to the Fourth Assessment Report of the Intergovernmental Panel on Climate Change*, edited by S. Solomon et al., pp. 847–940, Cambridge Univ. Press, New York.

Cumming, S. G. (2001), Forest type and wildfire in Alberta boreal mixedwood: What do fires burn?, *Ecol. Appl.*, *11*, 97–110, doi:10.1890/1051-0761(2001)011[0097:FTAWIT]2.0.CO;2.

Curry, J. A., W. B. Rossow, D. Randall, and J. L. Schramm (1996), Overview of the Arctic cloud and radiation characteristic, *J. Clim.*, *12*, 395–415.

Drobot, S. D., J. A. Maslanik, U. Herzfeld, and W. Wu (2006), Uncertainty in temperature and precipitation datasets over the WALE study region, *Earth Interact.*, *10*, 1–17, doi:10.1175/EI191.1.

Duffy, P. A., J. E. Walsh, J. M. Graham, D. H. Mann, and T. S. Rupp (2005), Impacts of large-scale atmospheric-ocean variability on Alaskan fire severity, *Ecol. Appl.*, *15*, 277–284, doi:10.1890/04-0739.

Dye, D. G. (2002), Variability and trends in the annual snow-cover cycle in Northern Hemisphere land areas, 1972–2000, *Hydrol. Process.*, *16*, 3065–3077, doi:10.1002/hyp.1089.

Euskirchen, E. S., et al. (2006), Importance of recent shifts in soil thermal dynamics on growing season length, productivity, and carbon sequestration in terrestrial high-latitude ecosystems, *Global Change Biol.*, *12*, 737–750, doi:10.1111/j.1365-2486.2006.01113.x.

Euskirchen, E. S., A. D. McGuire, and F. S. Chapin III (2007), Energy feedbacks of northern high-latitude ecosystems to the climate system due to reduced snow cover during 20th century warming, *Global Change Biol.*, *13*, 2425–2438, doi:10.1111/j.1365-2486.2007.01450.x.

Euskirchen, E. S., A. D. McGuire, F. S. Chapin III, S. Yi, and C. C. Thomspon (2009), Changes in vegetation in northern Alaska under scenarios of climate change 2003–2100: Implications for climate feedbacks, *Ecol. Appl.*, *19*, 1022–1043, doi:10.1890/08-0806.1.

Flannigan, M. D., K. A. Logan, B. D. Amiro, W. R. Skinner, and B. J. Stocks (2005), Future area burned in Canada, *Clim. Change*, *72*, 1–16, doi:10.1007/s10584-005-5935-y.

Geiger, R., R. A. Aron, and P. Todhunder (2009), *The Climate Near the Ground*, 7th ed., 623 pp., Rowan and Littlefield, New York.

Groisman, P. Y., T. R. Karl, and R. W. Knight (1994), Observed impact of snow cover on the heat balance and the rise of continental spring temperatures, *Science*, *263*, 198–200, doi:10.1126/science.263.5144.198.

Idso, S. B., and R. D. Jackson (1969), Thermal radiation from the atmosphere, *J. Geophys. Res.*, *74*, 5397–5403, doi:10.1029/JC074i023p05397.

Intergovernmental Panel on Climate Change (IPCC) (2000), *Emissions Scenarios: A Special Report of IPCC Working Group III*, edited by N. J. Nakicenovic et al., 599 pp., Cambridge Univ. Press, New York.

Johnstone, J. F., and F. S. Chapin III (2006), Effects of soil burn severity on post-fire tree recruitment in boreal forest, *Ecosystems*, *9*, 14–31, doi:10.1007/s10021-004-0042-x.

Johnstone, J. F., and E. S. Kasischke (2005), Stand-level effects of soil burn severity on postfire regeneration in a recently burned black spruce forest, *Can. J. For. Res.*, *35*, 2151–2163, doi:10.1139/x05-087.

Kasischke, E. S., and J. F. Johnstone (2005), Variation in fire severity and its effects on site conditions and post-fire succession in a black spruce forest complex in interior Alaska, *Can. J. For. Res.*, *35*, 2164–2177, doi:10.1139/x05-159.

Kasischke, E. S., and M. R. Turetsky (2006), Recent changes in the fire regime across the North American boreal region—Spatial and temporal patterns across Canada and Alaska, *Geophys. Res. Lett.*, *33*, L09703, doi:10.1029/2006GL025677.

Kasischke, E. S., D. Williams, and D. Barry (2002), Analysis of the patterns of large fires in the boreal forest region of Alaska, *Int. J. Wildland Fire*, *11*, 131–144, doi:10.1071/WF02023.

Kasischke, E. S., T. S. Rupp, and D. L. Verbyla (2003), Fire trends in the Alaskan boreal forest, in *Alaska's Changing Boreal Forest*, edited by F. S. Chapin III et al., pp. 285–301, Oxford Univ. Press, New York.

Kistler, R., et al. (2001), The NCEP-NCAR 50 year reanalysis: Monthly means CD-ROM and documentation, *Bull. Am. Meteorol. Soc.*, *82*, 247–267, doi:10.1175/1520-0477(2001)082<0247:TNNYRM>2.3.CO;2.

Kurz, W. A., C. C. Dymond, G. Stinson, G. J. Rampley, E. T. Neilson, A. L. Carroll, T. Ebata, and L. Safranyik (2008), Mountain pine beetle and forest carbon feedback to climate change, *Nature*, *452*, 987–990, doi:10.1038/nature06777.

Liu, H., and J. T. Randerson (2008), Interannual variability of surface energy exchange depends on stand age in a boreal forest fire chronosequence, *J. Geophys. Res.*, *113*, G01006, doi:10.1029/2007JG000483.

Liu, H., J. T. Randerson, J. Lindfors, and F. S. Chapin III (2005), Changes in the surface energy budget after fire in boreal ecosystems of interior Alaska: An annual perspective, *J. Geophys. Res.*, *110*, D13101, doi:10.1029/2004JD005158.

Lyons, E. A., Y. Jin, and J. T. Randerson (2008), Changes in surface albedo after fire in boreal forest ecosystems of interior Alaska assessed using MODIS satellite observations, *J. Geophys. Res.*, *113*, G02012, doi:10.1029/2007JG000606.

McGuire, A. D., and F. S. Chapin III (2006), Climate feedbacks in the Alaskan Boreal Forest, in *Alaska's Changing Boreal Forest*, edited by F. S. Chapin III et al., pp. 309–322, Oxford Univ. Press, New York.

McGuire, A. D., et al. (2008), The Western Arctic Linkage Experiment (WALE): Overview and synthesis, *Earth Interact.*, *12*, 1–13, doi:10.1175/2008EI239.1.

Mitchell, T. D., and P. D. Jones (2005), An improved method of constructing a database of monthly climate observations and associated high-resolution grids, *Int. J. Climatol.*, *25*, 693–712, doi:10.1002/joc.1181.

Nakićenović, N., and R. Swart (2000), *IPCC Special Report on Emissions Scenarios*, 612 pp., Cambridge Univ. Press, Cambridge, U. K.

New, M., D. Lister, M. Hulme, and I. Makin (2002), A high-resolution data set of surface climate over global land areas, *Clim. Res.*, *21*, 1–25, doi:10.3354/cr021001.

Parkinson, C. L., and W. M. Washington (1979), A large-scale numerical model of sea ice, *J. Geophys. Res.*, *84*, 311–337, doi:10.1029/JC084iC01p00311.

Payette, S. (1992), Fire as a controlling process in North American boreal forest, in *A Systems Analysis of the Global Boreal Forest*, edited by H. H. Shugart, R. Leemans, and G. B. Bonan, pp. 144–169, Cambridge Univ. Press, Cambridge, U. K.

Perovich, D. K., B. Light, H. Eicken, K. F. Jones, K. Runciman, and S. V. Nghiem (2007), Increasing solar heating of the Arctic Ocean and adjacent seas, 1979–2005: Attribution and role in the ice-albedo feedback, *Geophys. Res. Lett.*, *34*, L19505, doi:10.1029/2007GL031480.

Randerson, J. T., et al. (2006), The impact of boreal forest fire on climate warming, *Science*, *314*, 1130–1132, doi:10.1126/science.1132075.

Rupp, T. S., F. S. Chapin III, and A. M. Starfield (2000a), Response of subarctic vegetation to transient climatic change on the Seward Peninsula in northwest Alaska, *Global Change Biol.*, *6*, 541–555, doi:10.1046/j.1365-2486.2000.00337.x.

Rupp, T. S., A. M. Starfield, and F. S. Chapin III (2000b), A frame-based spatially explicit model of subarctic vegetation response to climatic change: A comparison with a point model, *Landscape Ecol.*, *15*, 383–400, doi:10.1023/A:1008168418778.

Rupp, T. S., F. S. Chapin III, and A. M. Starfield (2001), Modeling the influence of topographic barriers on treeline advance at the forest-tundra ecotone in northwestern Alaska, *Clim. Change*, *48*, 399–416, doi:10.1023/A:1010738502596.

Rupp, T. S., A. M. Starfield, F. S. Chapin III, and P. Duffy (2002), Modeling the impact of black spruce on the fire regime of Alaskan boreal forest, *Clim. Change*, *55*, 213–233, doi:10.1023/A:1020247405652.

Rupp, T. S., X. Chen, M. Oleson, and A. D. McGuire (2007), Sensitivity of simulated boreal fire dynamics to uncertainties in climate drivers, *Earth Interact.*, *11*, 1–21, doi:10.1175/EI189.1.

Starfield, A. M., and F. S. Chapin III (1996), Model of transient changes in arctic and boreal vegetation in response to climate and land use, *Ecol. Appl.*, *6*, 842–864, doi:10.2307/2269489.

Stocks, B. J., et al. (1998), Climate change and forest fire potential in Russian and Canadian boreal forests, *Clim. Change*, *38*, 1–13, doi:10.1023/A:1005306001055.

Stocks, B. J., M. A. Fosberg, M. B. Wotton, T. J. Lynham, and K. C. Ryan (2000), Climate change and forest fire activity in North American boreal forests, in *Fire, Climate Change, and Carbon Cycling in the Boreal Forest*, edited by E. S. Kasischke and B. J. Stocks, pp. 368–376, Springer, New York.

Stone, R. S., E. G. Dutton, J. M. Harris, and D. Longenecker (2002), Earlier spring snowmelt in northern Alaska as an indicator of climate change, *J. Geophys. Res.*, *107*(D10), 4089, doi:10.1029/2000JD000286.

Thompson, C. D., J. Beringer, F. S. Chapin III, and A. D. McGuire (2004), Relationship of structural complexity to land-surface energy exchange along a vegetation gradient from arctic tundra to boreal forest, *J. Veg. Sci.*, *15*, 397–406, doi:10.1111/j.1654-1103.2004.tb02277.x.

Turton, S. M. (1986), Solar radiation under cloudless skies, *Weatherwise*, *39*, 223–224.

Van Cleve, K., F. S. Chapin III, C. T. Dyrness, and L. A. Viereck (1991), State factor control of element cycling in Alaskan taiga forests, *BioScience*, *41*, 78–88, doi:10.2307/1311560.

Vörösmarty, C. J., B. M. Moore III, A. L. Grace, M. P. Gildea, J. M. Melillo, B. J. Peterson, E. B. Rastetter, and P. A. Steudler (1989), Continental scale models of water balance and fluvial transport: An application to South America, *Global Biogeochem. Cycles*, *3*, 241–265, doi:10.1029/GB003i003p00241.

Wang, X. J., and J. R. Key (2003), Recent trends in Arctic surface, cloud, and radiation properties from space, *Science*, *299*, 1725–1728, doi:10.1126/science.1078065.

Wang, X. J., and J. R. Key (2005), Arctic surface, cloud, and radiation properties based on the AVHRR Polar Pathfinder dataset. Part II: Recent trends, *J. Clim.*, *18*, 2575–2593, doi:10.1175/JCLI3439.1.

Welp, L. R., J. T. Randerson, and H. P. Liu (2007), The sensitivity of carbon fluxes to spring warming and summer drought depends on plant functional types in the boreal forest ecosystems, *Agric. For. Meteorol.*, *47*, 172–185, doi:10.1016/j.agrformet.2007.07.010.

Westerling, A. L., H. G. Hidalgo, D. R. Cayan, and T. W. Swetnam (2006), Warming and earlier spring increase western U.S. forest wildfire activity, *Science*, *313*, 940–943, doi:10.1126/science.1128834.

Wotton, B. M., and M. D. Flannigan (1993), Length of the fire season in a changing climate, *For. Chron.*, *69*, 187–192.

Wu, W., A. H. Lynch, S. Drobot, J. Maslanik, A. D. McGuire, and U. Herzfeld (2007), Comparative analysis of the western Arctic surface climate among observations and model simulations, *Earth Interact.*, *11*, 1–24, doi:10.1175/EI202.1.

Yarie, J. (1981), Forest fire cycles and life tables: A case study from interior Alaska, *Can. J. For. Res.*, *11*, 554–562, doi:10.1139/x81-076.

Zhuang, Q., et al. (2003), Carbon cycling in extratropical terrestrial ecosystems of the Northern Hemisphere during the 20th century: A modeling analysis of the influences of soil thermal dynamics, *Tellus, Ser. B*, *55*, 751–776.

F. S. Chapin III and E. S. Euskirchen, Institute of Arctic Biology, University of Alaska Fairbanks, Fairbanks, AK 99775, USA. (ffese@uaf.edu)

A. D. McGuire, Alaska Cooperative Fish and Wildlife Unit, U.S. Geological Survey, University of Alaska Fairbanks, Fairbanks, AK 99775, USA.

T. S. Rupp, Department of Forest Sciences, University of Alaska Fairbanks, Fairbanks, AK 99775, USA.

J. E. Walsh, International Arctic Research Center, University of Alaska Fairbanks, Fairbanks, AK 99775, USA.